

---

# Hierarchical Quantized Autoencoders

---

Will Williams<sup>\*1</sup> Sam Ringer<sup>\*1</sup> Tom Ash<sup>1</sup> John Hughes<sup>1</sup> David MacLeod<sup>1</sup> Jamie Dougherty<sup>1</sup>

## Abstract

Despite progress in training neural networks for lossy image compression, current approaches fail to maintain both perceptual quality and high-level features at very low bitrates. Encouraged by recent success in learning discrete representations with Vector Quantized Variational AutoEncoders (VQ-VAEs), we motivate the use of a hierarchy of VQ-VAEs to attain high factors of compression. We show that the combination of quantization and hierarchical latent structure aids likelihood-based image compression. This leads us to introduce a more probabilistic framing of the VQ-VAE, of which previous work is a limiting case. Our hierarchy produces a Markovian series of latent variables that reconstruct high-quality images which retain semantically meaningful features. These latents can then be further used to generate realistic samples. We provide qualitative and quantitative evaluations of reconstructions and samples on the CelebA and MNIST datasets.

## 1. Introduction

The internet age relies on lossy compression algorithms that transmit information at low bitrates. These algorithms are typically analysed through the rate-distortion trade-off, originally posited by Shannon (Shannon, 1959). However, a key issue with the trade-off is that for many applications the measure of distortion is only moderately correlated with the perceptual quality (or realism) of the reconstructed image (Blau & Michaeli, 2018; 2019), and methods that compress to extremely low rates tend to generate unrealistic images. Therefore, at these rates, methods that can balance *both* distortion and perceptual quality are of interest.

At low bitrates it is desirable to communicate only high-level concepts and offload the ‘filling in’ of details to a powerful decoder (Tschannen et al., 2018a). Flexible models such

as Neural Networks present a promising avenue to learn the complex transformations required to capture such high-level concepts (Santurkar et al., 2018; Gregor et al., 2016; Johnston et al., 2019). In this way, there is still significant scope to improve codecs by leveraging scalable learning-based approaches.

Requiring conceptually consistent and realistic reconstructions also has implications for representation learning (Tschannen et al., 2018b). If reconstructions or samples are always realistic, one can gain more confidence that a latent space has been learnt where the axes of variation span exclusively conceptual categories. Although not the primary focus of this work, such a structured latent space has the potential to improve sample complexity and learning in downstream supervised tasks, particularly if the latent variables capture valuable high-level concepts.

Variational Autoencoders (VAEs, Kingma & Welling 2014) are latent variable Neural Network models that have made significant strides in lossy-image compression (Theis et al., 2019; Agustsson et al., 2017). However, due to a combination of a poor likelihood function and a sub-optimal variational posterior (Rezende & Viola, 2018; Zhang et al., 2019), reconstructions can look blurred and unrealistic (Zhao et al., 2017a; Higgins et al., 2017).

Solutions to this problem then take two forms: either augmenting the likelihood model, for instance, by using adversarial methods (Tschannen et al., 2018a) or improving the structure of the posterior/latent space (Zhang et al., 2019; Alemi et al., 2018). However, at low rates both solutions struggle to match the realism of implicit generative models (Goodfellow et al., 2014). In addition to these problems, VAEs can be difficult to train, often due to *posterior collapse* (Lucas et al., 2019a), where the decoder ignores the latent variables during learning.

To address these issues, we introduce<sup>1</sup> the ‘Hierarchical Quantized Autoencoder’ (HQA), a novel hierarchical vector-quantized VAE that exploits structure in the codebook embedding spaces. We demonstrate that at low rates HQA produces reconstructions with higher perceptual quality than single and multi-layer equivalents. Moreover, the result-

---

<sup>\*</sup>Equal contribution      <sup>1</sup>Speechmatics, Cambridge, United Kingdom. Correspondence to: Will Williams <willw@speechmatics.com>, Sam Ringer <samr@speechmatics.com>.

---

<sup>1</sup>Code available at <https://github.com/speechmatics/hqa>

Table 1. CelebA interpolations of the HQA encoder output  $z_e$  in the 9 bit 8x8 latent space (171x compression). The original 64x64 images used in the interpolation are given on the left and right. The images in the middle are the resulting decoded images when using 8 linearly interpolated points between  $z_e$  generated by both images.



ing scheme admits scalable and stable training, whilst also capturing high level concepts.

The key idea behind HQA is leveraging hierarchically structured embedding spaces and a quantization scheme which forces reconstructions into the true data distribution. We elaborate on these ideas in Section 3.

Our key contributions are:

- We motivate the use of quantized hierarchies to improve the perceptual quality of reconstructions.
- When training quantized hierarchies, we show the importance of modelling a *distribution* over the previous discrete latent space, rather than compressing and reconstructing individual latent representations.
- We empirically show, using the MNIST and CelebA datasets, that HQAs can achieve low rate lossy compression, outperforming competing approaches on reconstruction FID and, in the case of MNIST, a downstream classification task.
- By interpolating between encoded representations of two images and decoding (Table 1), we show that the HQA latent space has dense support to create realistic samples across all values.

## 2. VQ-VAE

VQ-VAEs (Van Den Oord et al., 2017; Razavi et al., 2019) model high dimensional data  $x$  with a low-dimensional discrete latents  $z$ . A likelihood function  $p_\theta(x|z)$  is parameterized with a decoder that maps from latent space to observation space. A uniform prior distribution  $p(z)$  is defined over a discrete space of latent codes. As in the variational inference framework (Mnih & Gregor, 2014), an approximate

posterior is defined over the latents:

$$q_\phi(z = k|x) = \begin{cases} 1 & \text{for } k = \operatorname{argmin}_j \|z_e(x) - e_j\|_2 \\ 0 & \text{otherwise} \end{cases} \quad (1)$$

The codebook  $(e_i)_{i=1}^N$  enumerates a list of vectors and an encoder  $z_e(x)$  maps into latent space. A vector quantization operation then maps the encoded observation to the nearest code. During training the encoder and decoder are trained jointly to minimize the loss:

$$-\log p_\theta(x|z = k) + \|\operatorname{sg}[z_e(x)] - e_k\|_2^2 + \beta \|z_e - \operatorname{sg}[e_k]\|_2^2, \quad (2)$$

where  $\operatorname{sg}$  is a stop gradient operator. The first term is referred to as the *reconstruction loss*, the next term is the *codebook loss* and the final term is the *commitment loss*. In practice, the codes  $e_k$  are learnt via an online exponential moving average version of k-means.

## 3. Motivation For Quantized Hierarchies

Lossy compression schemes will invariably use some form of quantization to select codes for transmission. This section examines the behaviour of quantization-based models trained using maximum-likelihood. Using such a scheme, we aim to train a model to fit the true density shown in Figure 1a using only a single bit latent. Ideally, each of the four modes should be recovered, and no more, to guarantee both diverse and realistic samples.

### 3.1. Single Layer VQ-VAE

We begin by fitting a VQ-VAE with a 1-bit (2 code) latent to the density. The green trace of Figure 1b displays the resulting mode-covering behaviour. Mode-covering is a

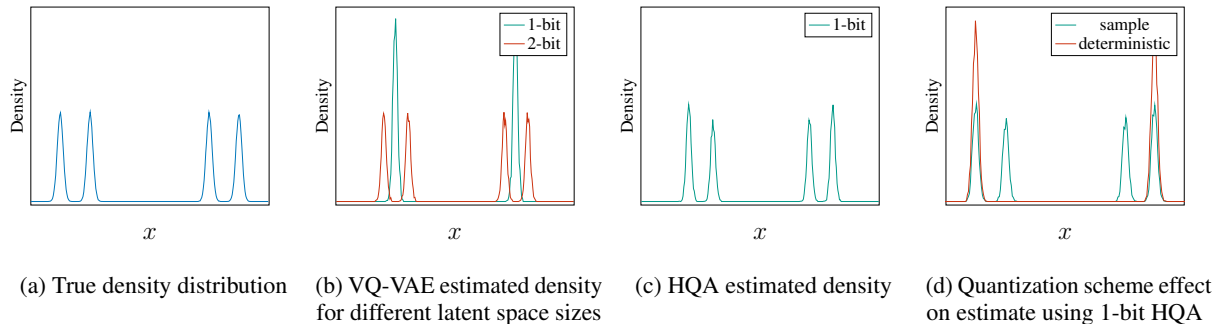


Figure 1. Motivation for quantized hierarchies using a simple data distribution

well known pathology of all likelihood-based models trained using the asymmetric divergence  $\text{KL}[p_\theta(x)||p(x)]$  (Lucas et al., 2019b). The mode-covering is expected as the number of codes is fewer than the number of input modes. However, a 2-bit latent space is expressive enough to model the input density and we observe a perfect fit, as shown in Figure 1b.

The question then arises: can we do better and fit the density perfectly with only a 1-bit latent?

### 3.2. Quantized Hierarchies

By training *another* 1-bit VQ-VAE on top of the pre-trained 2-bit model from above, a quantized hierarchy is formed.

The two layer system works as follows: a given datapoint is encoded by the bottom 2-bit layer. The result is then encoded by the top layer. After quantization, the result is decoded by the top layer, quantized again by the bottom layer before decoding through the bottom layer to the input space. This scheme is a simplification of the Hierarchical Quantized Autoencoder (HQA) described in depth in Section 4.2.

The reconstruction density produced by the full HQA scheme is shown in Figure 1c. The quantized hierarchy has successfully modelled the original density function and shows no mode-covering behaviour. Note the top level representation of this quantized hierarchy has the same information bottleneck as the original 1 bit VQ-VAE that failed to model the density function.

Each of the bottom layer’s 4 codes corresponds to a region of high density in the input space. Therefore, the single bit top layer will imperfectly model the latent space of the bottom layer for the same reasons that explain mode-covering. However, by quantizing the prediction of the top layer to a code of the bottom layer, the reconstructions will always fall in regions of high density in the input space.

This result shows that, under a given information bottleneck, quantized hierarchies allow for fundamentally different density modelling behaviour than equivalent single layer systems.

Therefore, we propose quantized hierarchies to mitigate the mode-covering behaviour shown by likelihood-based systems for the following reasons:

- **Hierarchy:** By choosing to model a distribution using a hierarchical latent space of increasingly compressed representations, mode-covering behaviour in the input space can be exchanged for mode-covering behaviour in the latent space. This also acts as a good meta-prior to match the hierarchical structure of natural data (Lázaro-Gredilla et al., 2016).
- **Quantization:** Quantization allows for the resolution of mode-covering behaviour in latent space, ensuring realistic reconstructions that fall in regions of high density in the input space.

### 3.3. Probabilistic Quantization

The example above can be further used to highlight a key subtlety of the quantization scheme used by VQ-VAE. VQ-VAE encoders output a deterministic posterior over codes, where the selected code is that closest to the encoder output. When mode covering is present in the latent space, this deterministic posterior will always select the same code. This results in mode dropping behaviour in the input space, as shown by the red trace in Figure 1d. This mode-dropping behaviour reduces reconstruction diversity.

However, by defining a stochastic posterior,  $q_\phi(z|x)$ , codes can be selected by sampling with probabilities that are a function of the distance between each code and the encoder output. This sampling operation preserves the full diversity of the input distribution, as shown by the blue trace in Figure 1d.

## 4. Method

### 4.1. Stochastic Posterior

A single layer of HQA differs from the VQ-VAE as it defines a stochastic posterior distribution over the codes. It models the approximate posterior probability  $q(z|x)$  as:

$$q(z = k|x) \propto \exp -\|z_e(x) - e_k\|_2^2. \quad (3)$$

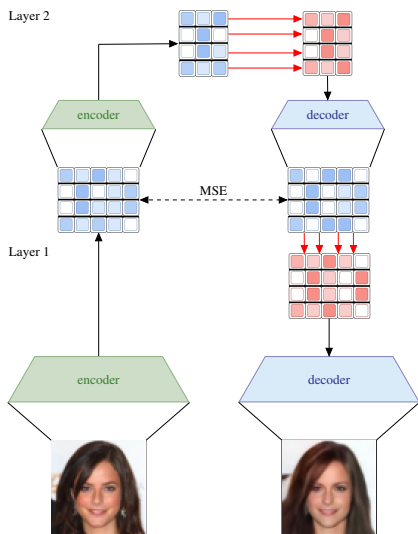


Figure 2. System diagram of a 2-layer HQA. Images are encoded into a continuous latent vector by Layer 1 before being encoded further by Layer 2. This representation is then quantized according to the stochastic posterior given by the red arrows, this is then decoded by Layer 2. If training, an MSE loss is taken with this output and the input to the Layer 2 encoder. If performing a full reconstruction, the representation is quantized and then decoded by Layer 1 to obtain the reconstruction.

This stochastic posterior leads to higher reconstruction diversity as discussed in Section 3.

Under this posterior,  $z_e$  must be positioned well relative to *all* codes in the latent space, not just the nearest code. As  $z_e$  defines a distribution over all codes, it carries more information about  $x$  than a single quantized latent sampled from  $q(z|x)$ . This is exploited by the HQA hierarchy, as discussed in the next section.

## 4.2. Hierarchical Quantized Autoencoders

The analysis in Section 3 suggests the use of a hierarchical sequence of discrete latent variables. Extended to multiple layers, this leads to the following observation model:

$$p(x|z_L) = p(x|z_1) \prod_{i=1}^{L-1} p(z_i|z_{i+1})p(z_L). \quad (4)$$

where  $z_i$  is the latent representation at layer  $i$  in a hierarchy of size  $L$ . Note this factorization shows a Markov relationship between the latent variables.

For hierarchical VQ-VAEs, an obvious choice when training higher layers is having the decoder parameterize a categorical distribution over possible codes of the previous layer. This can be trained with a categorical cross entropy between this distribution and the true code. Prior work on hierarchical VQ-VAEs has taken this approach (De Fauw et al., 2019).

Contrary to this approach, a *key finding* of this work is higher

layers that directly estimate the encoder output,  $z_e$ , of the previous layer - when trained with a mean-squared error loss (MSE) - leads to significantly improved performance.

As mentioned in the previous section, the embedding  $z_e$  implicitly represents a distribution over codes. By training higher layers to minimize the MSE between  $z_e$  from the layer below and an estimate  $\hat{z}_e$ , the higher layer learns to reconstruct a distribution over codes, not just a sample from this distribution, as in the naive cross-entropy scheme described above. Empirically, the results in Section 5.2 show this leads to large boosts in reconstruction quality.

When training HQA, we empirically found that constraining the encoders of each layer, and the decoders of the higher layers using a tanh activation function led to more stable training and improved performance. The final algorithm is described in Appendix D.

## 4.3. Greedy Training

An additional benefit of our scheme’s Markov structure is that each layer of HQA can be trained in a greedy sequential manner. Training each layer separately leads to lower memory footprints. We found the time until convergence when all layers were trained simultaneously was moderately less than greedy training. However, we preferred the increased flexibility of greedy training as it led to faster cycles of iteration.

## 4.4. Gaussian Mixture Model Interpretation

In a single layer model, the posterior probabilities over codes are proportional to the squared exponential negative distance to the encoder output. This model can therefore be interpreted as placing a Gaussian Mixture Model (GMM) in a continuous latent space. The Bayesian network for this model is given in Figure 3a, giving rise to the loss:

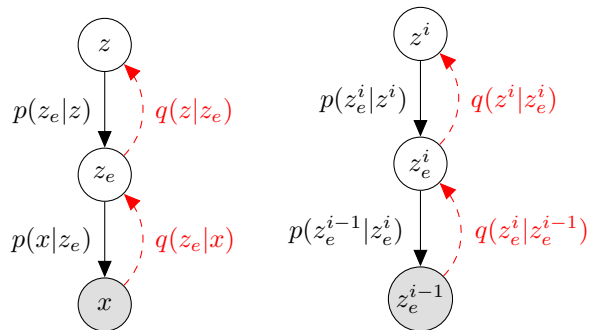
$$-\log p(x|z = k) - \mathcal{H}[q(z|x)] + \mathbb{E}_{q(z|x)} \|z_e(x) - e_z\|_2^2. \quad (5)$$

The first term is the reconstruction loss as in a normal VQ-VAE. The next is the entropy of  $q(z|x)$  that penalizes the posterior from being far from the uniform prior distribution  $p(z)$ . The final term is then similar to the codebook/commitment loss given in Equation 2 but instead taken over all codes, weighted by their probability. A derivation for the loss in Equation 5, based on the Evidence Lower Bound (ELBO), is given in Appendix B.

Under this interpretation, an Expectation Maximisation (EM) algorithm can be applied to learn codes through an exponential moving average, as in Van Den Oord et al. 2017. In practice, we do not take this approach and instead opt to learn codes directly using the loss in Equation 5 and additional techniques introduced in Section 4.6.

One often quoted benefit of using a VQ-VAE over a VAE is





(a) A single layer Deep Gaussian Mixture Model (b) The  $i^{\text{th}}$  layer of the hierarchy, reconstructing  $z_e^{(i-1)}$

Figure 3. Bayesian networks describing HQA, we include inference distributions in red. Figure (b) generalizes (a) when considering higher layers.

the use of a constant KL term which removes the problem of posterior collapse. However, Equation 5 has a non-constant entropy term, so this possibility is re-introduced. However, this is mitigated by multiplying the entropy term by a discount factor (Higgins et al., 2017; Alemi et al., 2018).

#### 4.5. Gumbel Softmax

During training, we sample from the stochastic posterior  $q(z|x)$  using the Gumbel Softmax relaxation (Jang et al., 2017; Maddison et al., 2017). This gives rise to a low variance approximation of gradients and has shown prior success in modelling discrete latent variables (Sønderby et al., 2017).

In addition, the extent of the continuous relaxation can be controlled with a temperature parameter  $\tau$ . Whilst training the HQA  $\tau$  is decayed linearly to 0 so that the Gumbel softmax more closely represents hard quantization, which is required when compressing to a fixed rate.

#### 4.6. Codebook Optimization

The codes are now directly learnt using the loss in Equation 5. This introduces a new pathology wherein codes that are assigned low probability under  $q(z|x)$  for all  $x$  receive low magnitude gradients, limiting the learning of that code’s embedding. The code will therefore continue to be assigned low probability under the posterior during training. We refer to these as ‘dead codes’ which result in sub-optimal compression as the effective rate is constrained by the number of codes in use.

By tracking the usage of each code during training we are able to identify the ‘dead codes’ and then reinitialize them near codes of high usage. This results in significantly higher effective rates during training, which leads to a more potent compression scheme.

In addition to this, we initialize more codes than the desired final amount and prune away underutilized codes during training.

Both code resetting and code pruning mirror prior work in online GMM training (Pinto & Engel, 2015; Verbeek et al., 2003) and over-parameterized latent spaces (Xu et al., 2018).

## 5. Experiments

### 5.1. CelebA

To show the scalability of HQA and the compression rates it can achieve on natural images, we train on the CelebA dataset (Liu et al., 2015) at a 64x64 resolution. The resulting system is a 7-layer HQA, where each layer has a codebook size of 512.

The first layer of the HQA system encodes the 64x64 input image into a 64x64 latent representation. For a codebook of size 512 (9 bits), this latent representation has capacity  $64 \times 64 \times 9 = 36,864$  bits. Each subsequent layer of HQA compresses the latent representation from the previous layer by a factor of 2 in each dimension. Therefore, after 7 HQA layers, the original 64x64 image is encoded to a  $1 \times 1 \times 9 = 9$  bit representation. As the input image is an 8-bit RGB image, at the final layer the compression ratio is then  $(64 \times 64 \times 8 \times 3) \div 9 = 10,923$ .

For comparison we also train 7 different VQ-VAE systems. Each VQ-VAE has the same compression ratio and approximate parameter count as its HQA equivalent. We also compare against the hierarchical quantized system introduced by De Fauw et al. 2019, which we abbreviate as ‘HAMs’. As with the VQ-VAE baselines, each HAMs layer has the same compression ratio as its HQA equivalent. We have chosen to compare against HAMs because their work closely resembles HQA in many respects, most notably, in their use of quantized hierarchies.

Table 2 shows reconstructions of two different input images from the test set for each layer of HQA, as well as the reconstructions from the VQ-VAE and HAM baselines.

The HQA reconstructions are more realistic than both VQ-VAE and HAM at all compression rates, with the difference becoming more exaggerated as the compression becomes more extreme. The high level features of the input image are also better preserved with HQA than with the baselines, even when the reconstructions are very different from the original in pixel space. This qualitative evaluation shows that using extreme compression, HQA produces realistic reconstructions that preserve semantically meaningful features, two of the key desiderata of extreme lossy compression.

For a quantitative comparison we also evaluate the test set

Table 2. Two reconstructed CelebA test-set images at different levels of compression for HQA, HAMs and VQ-VAE.

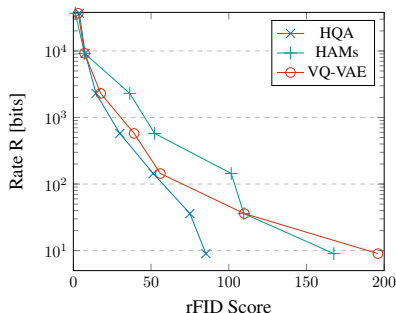
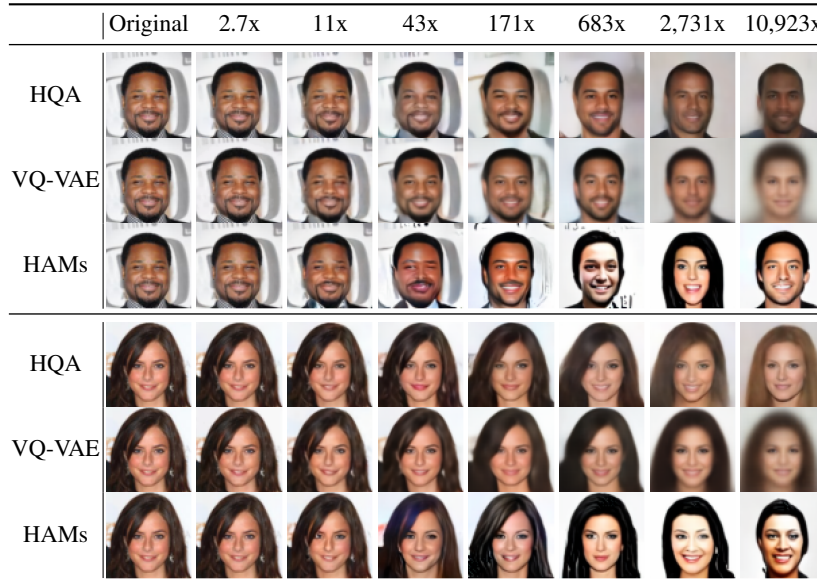


Figure 4. Plot of rate against reconstruction FID (rFID) for compressing and reconstructing CelebA test examples.

reconstruction Fréchet Inception Distance (rFID) for each layer of HQA, as well as for each of the baseline systems.

Figure 4 shows that HQA outperforms both VQ-VAE and HAMs at low compression rates. The difference becomes more pronounced as the compression becomes more extreme. This matches the qualitative results shown in Table 2.

## 5.2. MNIST Ablation Study

We performed an ablation study using the MNIST dataset (LeCun & Cortes, 2010), rescaled to 32x32. We began the ablation with a ‘VQ-VAE’ system and then introduce the notion of hierarchy with a ‘HAMs’ system. We then added either the ‘Direct’ scheme or Mean Squared Error (‘MSE’). ‘Direct’ refers to the combination of replacing k-means with direct code learning, code resetting and stochastic quantization using the Gumbel softmax (Section 4.5). ‘MSE’ also includes the tanh function as discussed in Section 4.2. Finally, we added ‘MSE’ and ‘Direct’ components together and then added two more stages - pruning of underused

codes (starting with 512 then pruning to 256) and the probabilistic loss (section 4.4).

We trained five layers, each compressing the original images by a factor of 2 in each dimension, such that the final layer compressed to a latent space of size 1x1. For VQ-VAE we trained to a 1x1 latent space directly. We used the same number of parameters ( $\sim 1M$ ) for each system and codebook size dimension 256 / 64. Compression was from 8192 ( $32 \times 32 \times 8$ ) down to 8 bits, compression ratio 1024.

For each system we compressed and reconstructed the 10k samples from the MNIST test set. We measured distortion (mean squared difference of reconstruction from source image), rFID (Heusel et al., 2017) between reconstructions and originals, and errors made by an MNIST classification system trained on original training images and tested on reconstructions. Points on rate curves were generated by using different layers of hierarchical models or training models with different compression rates for VQ-VAE.

Table 3 shows that for extreme compression to an 8-bit 1x1 latent space, the VQ-VAE base system gives best distortion figures and adding a hierarchy decreases performance. It also increases classification error which shows the reconstructions are less conceptually similar to the inputs. This initially implies that introducing a hierarchy of layers is leading to worse lossy compression. However, the rFID scores show that this is not the case. FID is a metric used to measure how similar groups of images are in terms of perceptual quality and adding a hierarchy gives a large improvement.

Across these metrics adding the ‘Direct’ and the ‘MSE’ components of HQA together gives large performance gains, but adding them individually does not. We believe this is be-

Table 3. Distortion, reconstruction FID (rFID) and Classification Error scores for ablated systems, after compressing MNIST images into an 8-bit 1x1 latent space then reconstructing. Reconstruction column shows reconstructions with the same source image in each vertical slice. ‘Direct’ covers introducing direct code learning, code resetting and quantization by sampling using the Gumbel softmax. ‘MSE’ means using Mean Squared Error loss on all layers and a tanh activation on outer layers.

System	Distortion ↓	rFID Score ↓	Class. Error (%) ↓	Reconstructions
No Compression	0.000	0.0	3.13	7 4 5 9 8
VQ-VAE	<b>0.039</b>	88.8	20.0	7 4 8 4 8
+ hierarchy (HAMs)	0.082	36.0	26.3	7 4 5 9 3
HAMs + Direct	0.107	34.5	54.5	7 3 2 4 8
HAMs + MSE	0.080	41.0	41.5	7 4 3 9 4
HAMs + Direct + MSE	0.056	31.8	13.7	7 4 5 9 8
+ code pruning	0.058	27.8	<b>13.1</b>	7 4 5 9 8
+ probabilistic loss ( <b>HQA</b> )	0.059	<b>26.5</b>	16.7	7 4 5 9 8

cause the MSE loss is better able to take advantage of the quantization sampling added in the ‘Direct’ components. The MSE loss cares more about position relative to all possible codes in latent space than cross entropy (which only cares about being near the one ‘correct’ code), and sampling when quantizing produces more meaning to this in latent space, by not always just snapping to the nearest code, but potentially mapping to any code with a probability related to its distance from that code. Without these components classification errors are very high, due to the intermediate systems being more prone to class switching.

Adding code pruning and the probabilistic loss on top gives the best rFID performance. These scores provide evidence that our system is creating more realistic images, even if the precise pixel values are no better matched to the originals. Figure 5 shows that these conclusions hold over a range of compression rates. HQA is the only system to give both good rFID and classification scores across all rates, the largest difference being at extreme compression rates.

The images in Table 3 show that under extreme compression the VQ-VAE systems reconstruct blurry images. They are achieving better distortion and classification scores by blurring, whereas our system is outputting sharper images that are more psychovisually ‘realistic’. In these images the HAMs system exhibits quite sharp but bold characters. The ablated aspects of our systems are visibly able to add more and more fine detail back into the images (albeit with class switching) until the final reconstructions from the full HQA system are sharp, realistic and semantically correct.

We created interpolations (Table 4) by mapping inputs to our embedding space, linearly interpolating, quantizing and decoding back to images. These show HQA has more dense support for coherent representations across the latent space than HAMs or VQ-VAE: intermediate images for HQA are sharp and coherently represent digits, with class swapping

Table 4. Interpolations of encoder output  $z_e$  in the 8 bit 1x1 latent space. The far left and right images are originals. Others are decoded from the interpolated encoder output  $z_e$ . Rows from top to bottom correspond to VQ-VAE, HAMs and HQA.

VQ-VAE	
HAMs	
HQA	

rather than deforming into unrealistic shapes. HAMs intermediate digits often degrade into less recognisable shapes; VQ-VAE intermediates are blurry and become amorphous.

Table 5. Interpolations generated for each layer in HQA. The far left and right images are originals. Others are decoded from the interpolated encoder output  $z_e$ . Bottom row (HQA-1) has a compression ratio of 4, each subsequent layer compresses by 4 again until the final layer (HQA-5) results in an 8 bit 1x1 latent space.

HQA-5	
HQA-4	
HQA-3	
HQA-2	
HQA-1	

Table 5 shows that HQA achieves this by fully utilising the hierarchy of layers available to it. Lower layers exhibit blurriness and overlapping versions of originals but as we ascend the layers we can see increasingly dense support is present to allow the intermediates to ‘snap’ to realistic and coherent looking digits from anywhere in the latent space.

These results combine to show that our system is able to maintain sharp images that are also semantically coherent under far harsher compression regimes than the systems we compared against.

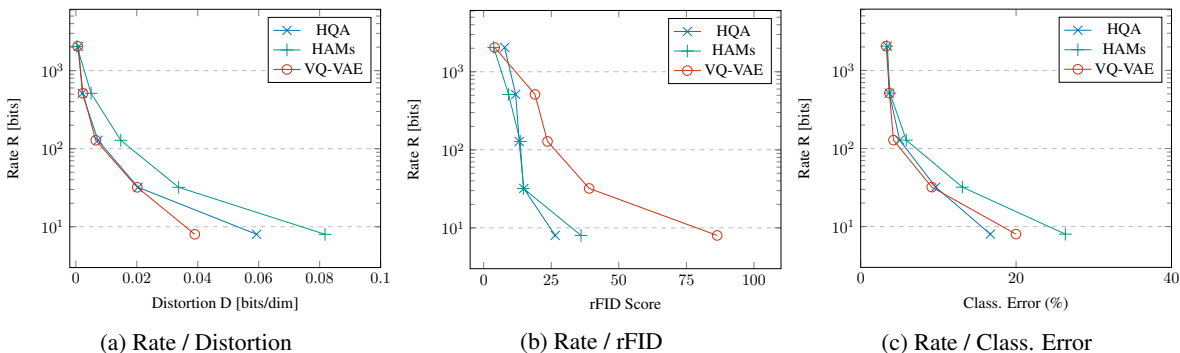


Figure 5. Plots of rate against distortion, reconstruction FID (rFID) and classification error for compressing and then reconstructing MNIST test examples.

## 6. Related Work

The problem of reconstructing realistic images in lossy compression is well known (Blau & Michaeli, 2018; Ballé et al., 2016). Attempts to remedy this with perceptual losses (Toderici et al., 2017; Ballé et al., 2018; Santurkar et al., 2018; Patel et al., 2019) have focused primarily on heuristically defined losses which capture different aspects of human-perceived perceptual quality.

Tschannen et al. 2018a attempt to address the same problem by introducing a distribution matching constraint, where the reconstructed samples are encouraged to follow the training data distribution.

Recent work (Ha & Schmidhuber, 2018) has found success in focusing the majority of modelling in latent space. In a similar spirit, Zhang et al. 2019 avoid both blurry samples and explicit perceptual losses by minimizing divergences in latent space rather than data space. Zhao et al. 2017c; Rezende & Viola 2018; Alemi et al. 2018 relax the KL penalty of the VAE to allow for a more flexible class of posteriors that don't require the model to blur images to achieve better distortions. Brekelmans et al. 2019 show that a more powerful noise model can aid lossy compression, with a focus on relaxing prior and marginal assumptions.

De Fauw et al. 2019; Razavi et al. 2019 train a hierarchy of VQ-VAEs for the purpose of using the discrete latents to train an autoregressive decoder (Van den Oord et al., 2016), whereas HQA has simple feed-forward decoders throughout. A hierarchical discrete VAE is trained using a Gumbel Softmax relaxation in (Liévin et al., 2019). Other hierarchies of VAEs are considered in (Sønderby et al., 2016; Zhao et al., 2017b) but these don't address the perceptual loss nor use the same Markov structure in latents. Additionally, (Maaløe et al., 2019) use skip connections between layers to propagate information.

Closely related to HQAs is Gregor et al. 2016, where a VAE-based hierarchy is constructed in an attempt to capture increasingly abstract concepts.

Different extensions to the VQ-VAE architecture have been suggested. Agustsson et al. 2017 use deterministic soft quantization in latent space and reduce this softness until full quantization is achieved.

Bornschein et al. 2017 use a trainable memory module much like a codebook but consider a slightly different generative model to the HQA. Sønderby et al. 2017 uses this memory interpretation and a sampling scheme much like the HQA's. Using mixture priors is previously studied in Dilokthanakul et al. 2016; Nalisnick et al. 2016; Tomczak & Welling 2018 where more expressive posteriors and generative models are considered.

## 7. Conclusion

In this work, we present the 'Hierarchical Quantized Autoencoder' (HQA), a viable method of training hierarchical VQ-VAEs for low rate semantic compression. To do this we use a stochastic posterior over codes which naturally motivates an MSE loss when training hierarchical layers. By incorporating a variety of additional improvements, we show HQA outperforms equivalent VQ-VAE architectures when reconstructing the CelebA and MNIST datasets under extreme compression.

## References

- Agustsson, E., Mentzer, F., Tschannen, M., Cavigelli, L., Timofte, R., Benini, L., and Van Gool, L. Soft-to-hard vector quantization for end-to-end learning compressible representations. In *Advances in Neural Information Processing Systems*, volume 2017-Decem, pp. 1142–1152, 2017.
- Alemi, A. A., Poole, B., Fische, I., Dillon, J. V., Saurous, R. A., and Murphy, K. Fixing a broken elbow. In *35th International Conference on Machine Learning, ICML 2018*, volume 1, pp. 245–265, 2018. ISBN 9781510867963.
- Ballé, J., Laparra, V., and Simoncelli, E. P. End-to-end



- optimization of nonlinear transform codes for perceptual quality. In *2016 Picture Coding Symposium (PCS)*, pp. 1–5. IEEE, 2016.
- Ballé, J., Minnen, D., Singh, S., Hwang, S. J., and Johnston, N. Variational image compression with a scale hyperprior. In *International Conference on Learning Representations, ICLR 2018 - Conference Track Proceedings*, 2018.
- Blau, Y. and Michaeli, T. The perception-distortion tradeoff. In *Proceedings of the IEEE Conference on Computer Vision and Pattern Recognition*, pp. 6228–6237, 2018.
- Blau, Y. and Michaeli, T. Rethinking lossy compression: The rate-distortion-perception tradeoff. *arXiv preprint arXiv:1901.07821*, 2019.
- Bornschein, J., Mnih, A., Zoran, D., and Rezende, D. J. Variational memory addressing in generative models. In *Advances in Neural Information Processing Systems*, volume 2017-Decem, pp. 3921–3930, 2017.
- Brekelmans, R., Moyer, D., Galstyan, A., and Ver Steeg, G. Exact rate-distortion in autoencoders via echo noise. In *Advances in Neural Information Processing Systems*, pp. 3884–3895, 2019.
- De Fauw, J., Dieleman, S., and Simonyan, K. Hierarchical autoregressive image models with auxiliary decoders. *arXiv preprint arXiv:1903.04933*, 2019.
- Dilokthanakul, N., Mediano, P. A., Garnelo, M., Lee, M. C., Salimbeni, H., Arulkumaran, K., and Shanahan, M. Deep unsupervised clustering with gaussian mixture variational autoencoders. *arXiv preprint arXiv:1611.02648*, 2016.
- Goodfellow, I., Pouget-Abadie, J., Mirza, M., Xu, B., Warde-Farley, D., Ozair, S., Courville, A., and Bengio, Y. Generative adversarial nets. In *Advances in Neural Information Processing Systems*, pp. 2672–2680, 2014.
- Gregor, K., Besse, F., Rezende, D. J., Danihelka, I., and Wierstra, D. Towards conceptual compression. In *Advances In Neural Information Processing Systems*, pp. 3549–3557, 2016.
- Ha, D. and Schmidhuber, J. World models. *arXiv preprint arXiv:1803.10122*, 2018.
- Heusel, M., Ramsauer, H., Unterthiner, T., Nessler, B., and Hochreiter, S. Gans trained by a two time-scale update rule converge to a local nash equilibrium. In *Advances in Neural Information Processing Systems*, pp. 6626–6637, 2017.
- Higgins, I., Matthey, L., Pal, A., Burgess, C., Glorot, X., Botvinick, M., Mohamed, S., and Lerchner, A. beta-vae: Learning basic visual concepts with a constrained variational framework. In *5th International Conference on Learning Representations, ICLR 2017 - Conference Track Proceedings*, 2017.
- Jang, E., Gu, S., and Poole, B. Categorical reparameterization with gumbel-softmax. In *5th International Conference on Learning Representations, ICLR 2017 - Conference Track Proceedings*, 2017.
- Johnston, N., Eban, E., Gordon, A., and Ballé, J. Computationally efficient neural image compression. *arXiv preprint arXiv:1912.08771*, 2019.
- Kingma, D. P. and Welling, M. Auto-encoding variational bayes. In *2nd International Conference on Learning Representations, ICLR 2014 - Conference Track Proceedings*, 2014.
- Lázaro-Gredilla, M., Liu, Y., Phoenix, D. S., and George, D. Hierarchical compositional feature learning. *arXiv preprint arXiv:1611.02252*, 2016.
- LeCun, Y. and Cortes, C. MNIST handwritten digit database. 2010. URL <http://yann.lecun.com/exdb/mnist/>.
- Liévin, V., Dittadi, A., Maaløe, L., and Winther, O. Towards Hierarchical Discrete Variational Autoencoders. Technical report, 2019.
- Liu, L., Jiang, H., He, P., Chen, W., Liu, X., Gao, J., and Han, J. On the variance of the adaptive learning rate and beyond. *arXiv preprint arXiv:1908.03265*, 2019.
- Liu, Z., Luo, P., Wang, X., and Tang, X. Deep learning face attributes in the wild. In *Proceedings of International Conference on Computer Vision (ICCV)*, December 2015. URL <http://mmlab.ie.cuhk.edu.hk/projects/CelebA.html>.
- Lucas, J., Tucker, G., Grosse, R., and Norouzi, M. Understanding posterior collapse in generative latent variable models. In *Deep Generative Models for Highly Structured Data, DGS@ICLR 2019 Workshop*, 2019a.
- Lucas, T., Shmelkov, K., Alahari, K., Schmid, C., and Verbeek, J. Adaptive density estimation for generative models. In Wallach, H., Larochelle, H., Beygelzimer, A., d’Alché Buc, F., Fox, E., and Garnett, R. (eds.), *Advances in Neural Information Processing Systems 32*, pp. 11993–12003. Curran Associates, Inc., 2019b. URL <http://papers.nips.cc/paper/9370-adaptive-density-estimation-for-generative-models.pdf>.
- Maaløe, L., Fraccaro, M., Liévin, V., and Winther, O. Biva: A very deep hierarchy of latent variables for generative modeling. In *Advances in Neural Information Processing Systems*, pp. 6548–6558, 2019.

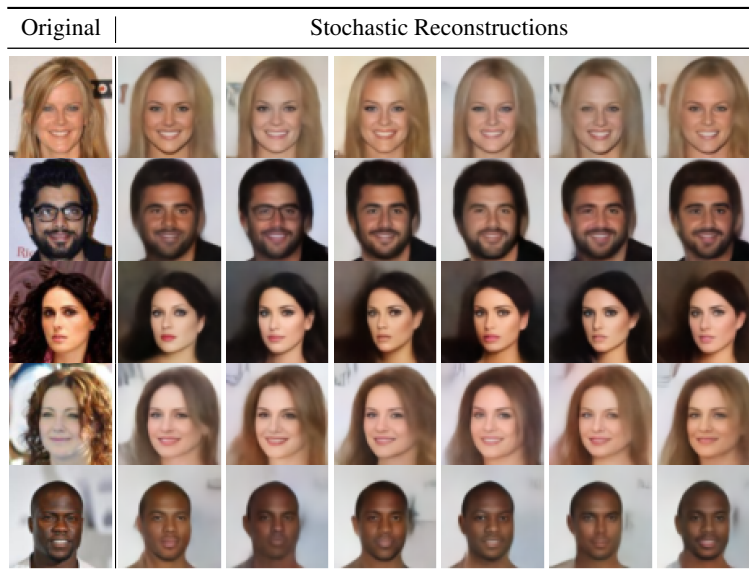
- Maddison, C. J., Mnih, A., and Teh, Y. W. The Concrete Distribution: A Continuous Relaxation of Discrete Random Variables. In *International Conference on Learning Representations*, 2017.
- Mnih, A. and Gregor, K. Neural variational inference and learning in belief networks. In *31st International Conference on Machine Learning, ICML 2014*, volume 5, pp. 3800–3809, 2014.
- Nalisnick, E., Hertel, L., and Smyth, P. Approximate inference for deep latent gaussian mixtures. In *NIPS Workshop on Bayesian Deep Learning*, 2016.
- Patel, Y., Appalaraju, S., and Manmatha, R. Deep perceptual compression. *arXiv preprint arXiv:1907.08310*, 2019.
- Pinto, R. C. and Engel, P. M. A fast incremental gaussian mixture model. *PLoS one*, 10(10):e0139931–e0139931, 2015.
- Razavi, A., van den Oord, A., and Vinyals, O. Generating diverse high-fidelity images with vq-vae-2. In *Advances in Neural Information Processing Systems 32*, pp. 14837–14847. Curran Associates, Inc., 2019.
- Rezende, D. J. and Viola, F. Taming vaes. *arXiv preprint arXiv:1810.00597*, 2018.
- Santurkar, S., Budden, D., and Shavit, N. Generative compression. In *2018 Picture Coding Symposium (PCS)*, pp. 258–262. IEEE, 2018.
- Shannon, C. E. Coding theorems for a discrete source with a fidelity criterion. 1959.
- Sønderby, C. K., Raiko, T., Maaløe, L., Sønderby, S. K., and Winther, O. Ladder variational autoencoders. In *Advances in Neural Information Processing Systems*, pp. 3738–3746, 2016.
- Sønderby, C. K., Poole, B., and Mnih, A. Continuous Relaxation Training of Discrete Latent Variable Image Models. *NIPS 2017 Bayesian Deep Learning Workshop*, 2017. URL <http://bayesiandeeplearning.org/2017/papers/54.pdf>.
- Theis, L., Shi, W., Cunningham, A., and Huszár, F. Lossy image compression with compressive autoencoders. In *5th International Conference on Learning Representations, ICLR 2017 - Conference Track Proceedings*, 2019.
- Toderici, G., Vincent, D., Johnston, N., Jin Hwang, S., Minnen, D., Shor, J., and Covell, M. Full resolution image compression with recurrent neural networks. In *Proceedings of the IEEE Conference on Computer Vision and Pattern Recognition*, pp. 5306–5314, 2017.
- Tomczak, J. M. and Welling, M. VAE with a vampprior. In *International Conference on Artificial Intelligence and Statistics, AISTATS 2018*, pp. 1214–1223, 2018.
- Tschannen, M., Agustsson, E., and Lucic, M. Deep generative models for distribution-preserving lossy compression. In *Advances in Neural Information Processing Systems*, pp. 5929–5940, 2018a.
- Tschannen, M., Bachem, O., and Lucic, M. Recent advances in autoencoder-based representation learning. *NeurIPS Workshop on Bayesian Deep Learning*, 2018b.
- Van den Oord, A., Kalchbrenner, N., Espeholt, L., Vinyals, O., Graves, A., et al. Conditional image generation with pixelcnn decoders. In *Advances in Neural Information Processing Systems*, pp. 4790–4798, 2016.
- Van Den Oord, A., Vinyals, O., and Kavukcuoglu, K. Neural discrete representation learning. In *Advances in Neural Information Processing Systems*, volume 2017-Decem, pp. 6307–6316, 2017.
- Verbeek, J. J., Vlassis, N., and Kröse, B. Efficient greedy learning of gaussian mixture models. *Neural computation*, 15(2):469–485, 2003.
- Xu, J., Hsu, D. J., and Maleki, A. Benefits of overparameterization with em. In *Advances in Neural Information Processing Systems*, pp. 10662–10672, 2018.
- Zhang, Z., Zhang, R., Li, Z., Bengio, Y., and Paull, L. Perceptual generative autoencoders. In *Deep Generative Models for Highly Structured Data, DGS@ICLR 2019 Workshop*, 2019. URL <https://github.com/zj10/PGA>.
- Zhao, S., Song, J., and Ermon, S. Towards deeper understanding of variational autoencoding models. *arXiv preprint arXiv:1702.08658*, 2017a.
- Zhao, S., Song, J., and Ermon, S. Learning hierarchical features from deep generative models. In *Proceedings of the 34th International Conference on Machine Learning-Volume 70*, pp. 4091–4099. JMLR. org, 2017b.
- Zhao, S., Song, J., and Ermon, S. Towards deeper understanding of variational autoencoding models. *arXiv preprint arXiv:1702.08658*, 2017c.

## A. Additional HQA Results

Table 6. Additional CelebA interpolations of the HQA encoder output  $z_e$  in the 9 bit 8x8 latent space (171x compression).



Table 7. CelebA reconstruction diversity when performing stochastic decodes from the 9 bit 4x4 latent space (683x compression).



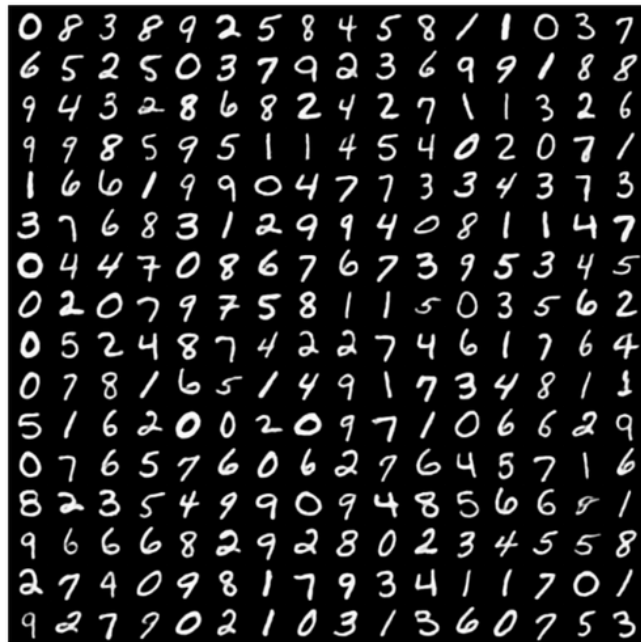


Figure 6. 'Free' samples obtained by exhaustively enumerating over all 256 codes from the 1x1 latent space of the trained MNIST HQA stack and decoding into pixel-space.

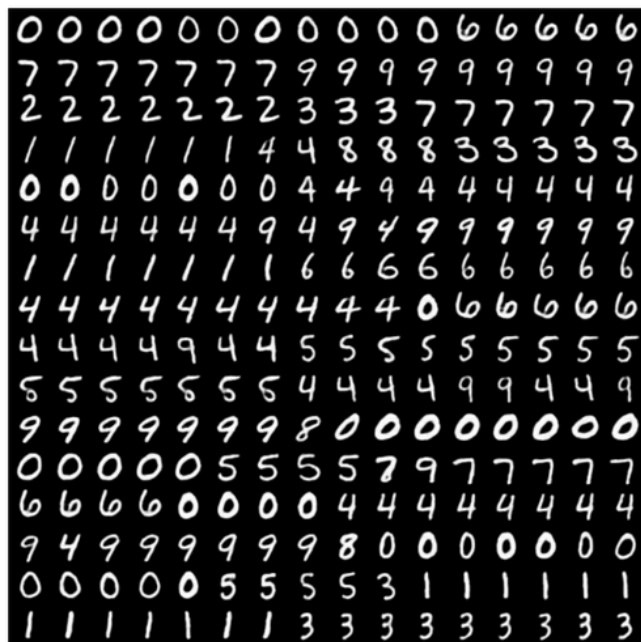


Figure 7. Rows show pairs of test images that have been encoded to the top of the HQA MNIST stack, interpolated across their codebook embeddings, quantized and then decoded.



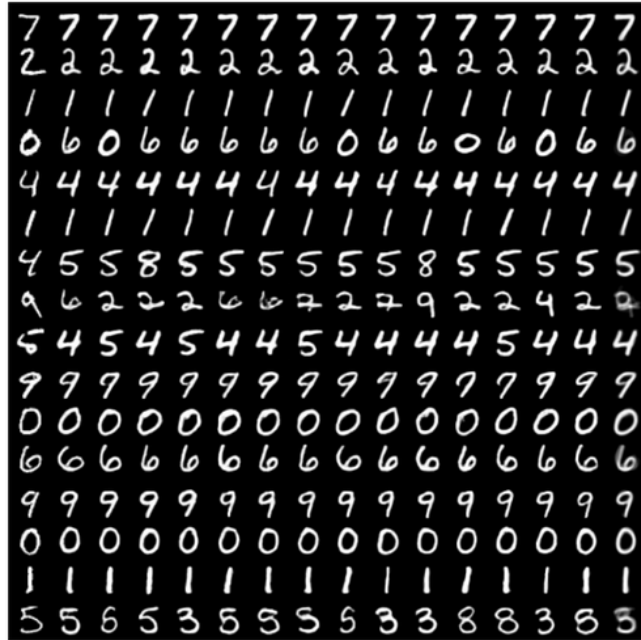


Figure 8. Each row displays the diversity of stochastic decoding for a different held out MNIST image. The first column is the original, then 14 columns of stochastic decodes, and then final column is the average image of 14 decodes. Class switching behaviour is displayed due to the high compression factor when going through the 1x1 latent bottleneck.

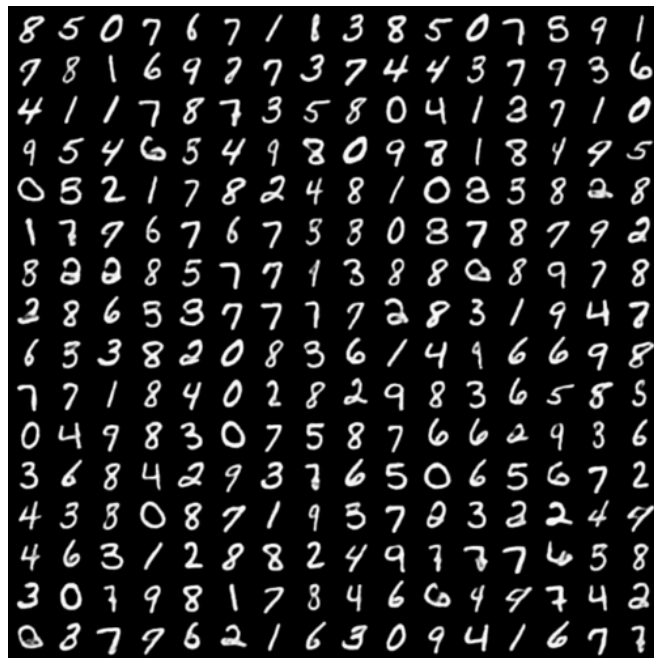


Figure 9. Samples generated by training a vanilla VAE on top of the learnt HQA 2x2 latent space and decoding first through the VAE then the HQA stack.

## B. Probabilistic VQ-VAE

### B.1. Motivation

In this section we outline the probabilistic model that motivates the HQA loss:

$$\mathcal{L} = -\log p(x|z = k) - \mathcal{H}[q(z|x)] + \mathbb{E}_{q(z|x)} \|z_e(x) - e_k\|_2^2. \quad (6)$$

A desired property of the HQA, motivated in Section 3.3 of the paper, is the non-deterministic posterior  $q(z|x)$  defined over codebook space. For the HQA, this is defined as a softmax with logits equal to the negative squared Euclidean distances between the encoded points ( $z_e(x)$ ) and codebook vectors ( $e_k$ ):

$$q(z = k|x) \propto \exp -\|z_e(x) - e_k\|_2^2. \quad (7)$$

This form of posterior occurs in a simple Gaussian Mixture Model (GMM), where they are referred to as *responsibilities*. In the GMM, the observed variables  $x'$  are generated from possible sources  $z' = 1, \dots, N$ . The responsibility of each source is then:

$$q(z' = k|x') \propto \exp -\|x' - e_k\|_2^2. \quad (8)$$

This mirrors Equation 7 where the encoded point  $z_e(x)$  is replaced by the observations  $x'$ . Therefore, in order to derive a Evidence LOWER Bound (ELBO) for our model, we use a small extension to the GMM that incorporates the encoder-decoder architecture.

### B.2. Probabilistic Model

We introduce an additional latent variable  $z_e$  into the standard GMM setup, so that the distribution  $p(x|z)$  factorizes as:

$$p(x|z) = \underbrace{p(x|z_e)}_{\text{Decoder}} \underbrace{p(z_e|z)}_{\text{GMM}}. \quad (9)$$

We contrast these two models in Figure 10. In this setup we treat  $z_e$  as being generated from a GMM.  $z_e$  is then fed through the decoder neural network.

To then infer a value for  $z$  we first approximate the posterior  $p(z_e|x)$  with a deterministic distribution on the output of the encoder neural network. To emphasize this in our analysis we refer to the output of the encoder as  $z_e(x)$ , whilst we refer to the latent variable as  $z_e$ . The final stage of inference to calculate  $p(z|z_e)$  reduces to a simple GMM model with observed variables  $x'$  in Equation 8 replaced with  $z_e(x)$ . This leads exactly to the posterior probabilities given in Equation 7. As  $q(z_e|x)$  is deterministic we have that  $q(z|z_e) = q(z|x)$  and so we use these expressions interchangeably.

This model is a Variational Autoencoder with a simple Mixture of Gaussians prior. In the prior, each Gaussian is assumed to be independent and have constant variance. Similar, more complex models are considered in (Dilokthanakul et al., 2016; Nalisnick et al., 2016; Tomczak & Welling, 2018).

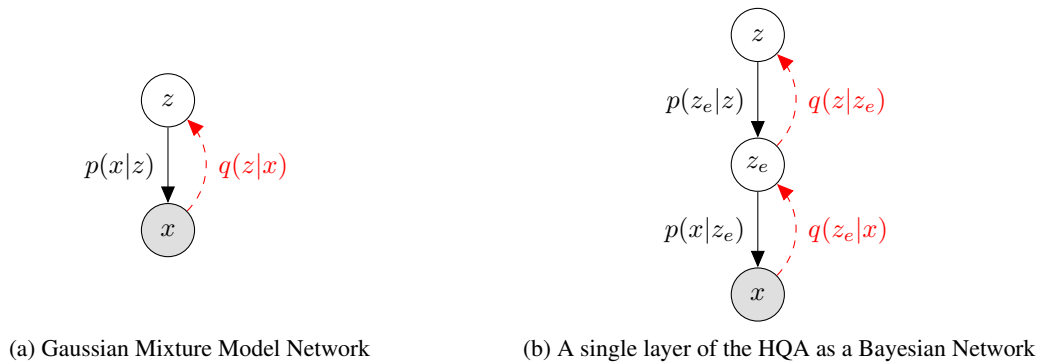


Figure 10. Contrasting the probabilistic model of a GMM and a single layer of the HQA

### B.3. Deriving the ELBO

Finally, as we have recovered the posterior probabilities we desire, we now derive the ELBO loss. For a general latent variable model with observation  $x$  this is formulated as:

$$\mathcal{L}_{\text{ELBO}} = \mathbb{E}_{q(z|x)} \log p_{\theta}(x|z) - \text{KL}[q(z|x)||p(z)] \quad (10)$$

where  $q(z|x)$  is our approximate posterior distribution. However, in our case we have two latent variables, giving the loss:

$$\mathcal{L}_{\text{ELBO}} = \mathbb{E}_{q(z, z_e|x)} \log p_{\theta}(x|z, z_e) - \text{KL}[q(z, z_e|x)||p(z, z_e)]. \quad (11)$$

We can then make use of the factorization in Equation 9 to rearrange this as:

$$\mathcal{L}_{\text{ELBO}} = \underbrace{\mathbb{E}_{q(z|z_e)q(z_e|x)} \log p_{\theta}(x|z_e)}_{\text{Reconstruction Loss}} - \underbrace{\text{KL}[q(z|z_e)q(z_e|x)||p(z)p(z_e|z)]}_{\text{KL to prior}}. \quad (12)$$

We now consider each of these terms separately.

#### B.3.1. PRIOR KL LOSS

The Prior KL Loss is given by:

$$\mathcal{L}_{\text{prior}} = \text{KL}[q(z|z_e)q(z_e|x)||p(z)p(z_e|z)]. \quad (13)$$

This factorizes into two separate KL terms

$$\mathcal{L}_{\text{prior}} = \text{KL}[q(z|x)||p(z)] + \mathbb{E}_{q(z|x)} \text{KL}[q(z_e|x)||p(z_e|z)]. \quad (14)$$

As we define a uniform prior over mixture parameters  $p(z)$ , the first term becomes the entropy term  $\mathcal{H}(q(z|x))$  as given in Equation 6. The next term is then:

$$\mathbb{E}_{q(z|x)} \text{KL}[q(z_e|x)||p(z_e|z)] = -\mathbb{E}_{q(z|x)} \log \left( e^{-\|z_e(x) - e_z\|_2^2} \right) = \mathbb{E}_{q(z|x)} \|z_e(x) - e_z\|_2^2 \quad (15)$$

which is the final part of Equation 6. We omit two details: the constant terms and the factor of 0.5 multiplied by the variance that usually occurs in the Gaussian density function as this is reweighted before training.

#### B.3.2. RECONSTRUCTION LOSS

The reconstruction loss is given by:

$$\mathcal{L}_{\text{recon}} = \mathbb{E}_{q(z|z_e)q(z_e|x)} \log p_{\theta}(x|z_e) = \mathbb{E}_{q(z_e|x)} \mathbb{E}_{q(z|z_e)} \log p_{\theta}(x|z_e). \quad (16)$$

In order to train with the quantized behaviour we require, we don't follow this calculation when calculating the reconstruction loss. Instead we sample from  $q(z|z_e(x))$  and feed this back through the decoder. This modification gives

$$\mathcal{L}'_{\text{recon}} = \log p(x|z_e = k) \quad (17)$$

where  $k$  is sampled from  $q(z|z_e(x))$ . To clarify, whilst training, instead of using the encoded point  $z_e$  as the input to the decoder, we feed the codebook vector sampled from the posterior  $q(z|x)$ .

### B.4. VQ-VAE as a limiting case

If we include a temperature parameter in our softmax posterior

$$q(z = k|x) \propto \exp \left( -\frac{1}{\tau} \|z_e(x) - e_k\|_2^2 \right) \quad (18)$$

then as  $\tau \rightarrow 0$ , the posterior converges to a deterministic distribution:

$$q(z = k|x) = \begin{cases} 1 & \text{for } k = \text{argmin}_j \|z_e(x) - e_j\|_2 \\ 0 & \text{otherwise} \end{cases} \quad (19)$$

This is precisely the posterior that arises in the VQ-VAE. In addition, the KL prior terms then become:

$$\mathcal{H}(q(z|x)) = 0 \quad (20)$$

$$\mathbb{E}_{q(z|x)} \|z_e(x) - e_z\|_2^2 = \|z_e(x) - e_k\|_2^2 \quad (21)$$

If then stop gradient operators are applied to (21), the commitment and codebook loss from the VQ-VAE are recovered.

## C. Architecture, training and hyper-parameters

### C.1. HQA

Each layer in the HQA stack is composed of an encoder, decoder and vector quantization layer. Encoders and decoders are feed forward networks composed of convolutional layers with 3x3 filters. Optional dilated convolutions are used in the decoder to increase the decoder’s receptive field. Each code in the VQ layer codebook is represented by a 64 dimensional vector. A tanh activation was applied to the outputs of encoder and decoder for all layers apart from layer 1, where a sigmoid activation was applied to the output of the decoder. This was found to constrain the embedding space and improve performance of higher level layers.

The downsampling needed for compression is achieved through a strided convolution in the encoder and upsampling through nearest neighbour interpolation in the decoder. Each HQA layer is trained greedily with an MSE loss; gradients are only back-propagated through that single layer. For the first layer, the loss is taken between input pixels and decoder outputs, while all other layers calculate the loss between the input embedding  $z_e$  and the predicted  $\hat{z}_e$ .

Optimization is performed using RAdam (Liu et al., 2019) with a learning rate of 4e-4 which is cosine annealed in the final third of training. Each layer was trained with distributed training across 8 Nvidia TITAN RTX’s for CelebA, whilst MNIST was trained on a single TITAN X. During training, the Gumbel softmax temperature is linearly annealed to 0.01, with an initial temperature of 0.4 and 0.66 for CelebA and MNIST respectively.

	CelebA							MNIST				
	L1	L2	L3	L4	L5	L6	L7	L1	L2	L3	L4	L5
Input size	64	64	32	16	8	4	2	32	16	8	4	2
Batch size	128	128	128	128	128	128	128	512	512	512	512	512
Encoder layers	3	3	3	3	3	3	3	3	3	3	3	3
Decoder layers	6	6	6	6	6	6	6	3	3	3	3	3
Encoder hidden units	64	64	512	512	512	512	512	16	16	32	48	80
Decoder hidden units	64	64	512	512	512	512	512	16	32	48	80	128
Codebook size	512	512	512	512	512	512	512	256	256	256	256	256
$\beta_e$ (entropy loss coefficient)	5e-5	1e-3	1e-3	1e-3	1e-3	1e-3	1e-3	1e-3	1e-3	1e-3	1e-3	1e-3
$\beta_c$ (commitment loss coefficient)	5e-5	1e-3	1e-3	1e-3	1e-3	1e-3	1e-3	1e-3	1e-3	1e-3	1e-3	1e-3
Training steps	100k	100k	100k	100k	60k	60k	60k	18k	18k	18k	18k	18k

Table 8. Hyper parameters of HQA network used for CelebA and MNIST experiments

### C.2. HAMs

The implemented HAMs architecture follows De Fauw et al. 2019. Notably, it implements an MSE loss on pixels but all other layers use cross entropy for the reconstruction term. Separate commitment and codebook loss terms are also used. The codebook is not learnt directly, but updated via an online exponential moving average version of k-means.

	CelebA							MNIST				
	L1	L2	L3	L4	L5	L6	L7	L1	L2	L3	L4	L5
Input size	64	64	32	16	8	4	2	32	16	8	4	2
Batch size	32	64	64	64	64	64	64	512	512	512	512	512
Encoder conv layers	3	3	3	3	3	3	3	3	3	3	3	3
Decoder conv layers	3	3	3	3	3	3	3	3	3	3	3	3
Encoder hidden units	64	80	256	256	256	256	512	16	16	32	48	80
Decoder hidden units	64	80	512	512	512	512	512	16	26	40	58	96
Encoder residual blocks	2	2	2	3	3	2	1	0	0	0	0	0
Decoder residual blocks	2	2	2	3	3	2	1	0	0	0	0	0
Codebook size	512	512	512	512	512	512	512	256	256	256	256	256
$\beta$ (commitment loss coefficient)	1	50	50	50	50	50	10	0.02	0.02	0.02	0.02	0.02
Learning rate	4e-4	4e-4	4e-4	4e-4	1e-4	1e-4	1e-4	4e-4	4e-4	4e-4	4e-4	4e-4
Training steps	250k	300k	50k	50k	50k	50k	25k	18k	18k	18k	18k	18k

Table 9. Hyper parameters of HAMs network used for CelebA and MNIST experiments



### C.3. VQ-VAE

The implemented VQ-VAE architecture is comparable to HAMS, with the noticeable exception that there is no hierarchy. The same compression rates are achieved through downsampling multiple times. The entire network is trained end-to-end as a single layer, instead of greedily with local losses. The layers denoted in the table below refer VQ-VAE systems with equivalent compression factors to the same HQA and HAM layers. In all instances predictions are made in pixel space. The residual block implementation is based on the original VQ-VAE [Van Den Oord et al. 2017](#).

	CelebA							MNIST				
	L1	L2	L3	L4	L5	L6	L7	L1	L2	L3	L4	L5
Input size	64	64	32	16	8	4	2	32	16	8	4	2
Batch size	32	64	64	64	64	64	64	512	512	512	512	512
Encoder conv layers	2	3	4	5	6	7	8	2	3	4	5	6
Decoder conv layers	3	4	5	6	7	8	9	3	4	5	6	7
Encoder hidden units	64	80	256	256	384	400	512	22	40	50	62	78
Decoder hidden units	64	80	256	512	512	512	512	16	18	20	22	22
Encoder residual blocks	2	3	4	4	4	4	2	0	0	0	0	0
Decoder residual blocks	2	3	4	4	4	4	2	0	0	0	0	0
Codebook size	512	512	512	512	512	512	512	256	256	256	256	256
$\beta$ (commitment loss coefficient)	0.05	0.25	0.25	0.25	0.25	0.25	0.25	0.125	0.125	0.125	0.125	0.125
Learning rate	4e-5	4e-5	4e-5	1e-4	1e-4	1e-4	1e-4	4e-4	4e-4	4e-4	4e-4	4e-4
Training steps	250k	250k	250k	150k	150k	150k	50k	18k	18k	18k	18k	18k

Table 10. Hyper parameters of VQ-VAE network used for CelebA and MNIST experiments

### C.4. Codebook Resetting & Pruning

**Resetting:** During training, the total number of times that  $z_e$  is quantized to each code is accumulated over 20 batches. After these 20 batches, the most and least used code,  $e_m$  and  $e_l$  respectively, are found. If the usage of  $e_l$  is less than 3% than that of  $e_m$ , the position of  $e_l$  is reset such that  $e_l := e_m + \epsilon$  where  $\epsilon \sim N(0, 0.01)$ . This scheme is activate for the first 75% of training.

**Pruning:** For the MNIST experiments, we utilized code pruning. Each codebook was initialised with 512 codes and every 40 batches the least used code was removed, reducing the total number of codes in the codebook by one. This scheme remains activate until the remaining number of codes in the codebook reached 256, the desired final value.

## D. Algorithm description

---

### Algorithm 1 HQA Training

---

```

1:  $e$ : codebook embeddings,  $e_k$ : embdding for code  $k$ ,  $N$ : number of codes in each layer
2:  $L$ : number of layers in stack
3:  $\theta_i \leftarrow$  Initialize network parameters for encoders ( $Encoder_i$ ) and decoders ( $Decoder_i$ )  $\forall i \in L$ 
4: for  $l$  in  $1, \dots, L$  do ▷ Train each layer greedily
5:    $\tau \leftarrow 0.4$  ▷ Set initial codebook temperature
6:   while not converged do
7:      $X \leftarrow$  Random minibatch
8:     if  $l = 1$  then
9:        $z_{e-lower} \leftarrow X$ 
10:    else
11:       $z_{e-lower} \leftarrow Encoder_{0..l-1}(X)$  ▷ Encode up through pre-trained lower layers - no quantization
12:    end if
13:     $z_e \leftarrow Encoder_l(z_{e-lower})$ 
14:     $p(k|z_e) = \exp(-\frac{1}{2}\|z_e - e_k\|_2^2) / \sum_{i=1}^N \exp(-\frac{1}{2}\|z_e - e_i\|_2^2)$  ▷ Distribution over codes
15:    softonehot  $\sim$  RelaxedCategorical( $\tau, p(k|z_e)$ ) ▷ Reparameterized Gumbel-softmax sample
16:     $z_{q-soft} \leftarrow$  softonehot  $\ast e$  ▷ Soft quantized codebook lookup
17:     $\hat{z}_{e-lower} \leftarrow Decoder_l(z_{q-soft})$ 
18:     $\mathcal{L}'_{recon} = (\hat{z}_{e-lower} - z_{e-lower})^2$ 
19:     $\mathcal{L}_{entropy} = \sum_k p(k|z_e) \log p(k|z_e)$ 
20:     $\mathcal{L}_{commit} = \sum_k p(k|z_e) \|z_e - e_k\|_2^2$ 
21:     $\theta_i \leftarrow \theta_i - \eta \nabla_{\theta_i} (\mathcal{L}'_{recon} + \beta_e \mathcal{L}_{entropy} + \beta_c \mathcal{L}_{commit})$ 
22:     $\tau \leftarrow anneal(\tau)$  ▷ Anneal linearly
23:  end while
24: end for

```

---

### Algorithm 2 HQA Reconstruction via Ancestral Sampling

---

```

1:  $e$ : codebook embeddings
2:  $L$ : number of layers in stack
3: Trained encoders ( $Encoder_i$ ) and decoders ( $Decoder_i$ )  $\forall i \in L$ 
4:  $x$ : Datapoint to reconstruct
5:  $z_e \leftarrow Encoder_{0..l}(x)$ 
6: for  $l$  in  $L, \dots, 1$  do
7:    $p(k|z_e) = \exp(-\frac{1}{2}\|z_e - e_k\|_2^2) / \sum_{i=1}^N \exp(-\frac{1}{2}\|z_e - e_i\|_2^2)$  ▷ Distribution over codes
8:   onehot  $\sim p(k|z_e)$ 
9:    $z_q \leftarrow$  onehot  $\ast e$  ▷ Hard-quantized codebook lookup
10:   $z_e \leftarrow Decoder_l(z_q)$ 
11: end for
12: return  $z_e$ 

```

---

Note that for hard reconstructions at fixed rates, we do not necessarily need to perform hard-quantized codebook lookups except on the very top codebook. For simplicity, and to provide a single hierarchy where each layer can provide compression at a fixed rate, we anneal the temperature close to zero and at test time always perform hard quantization operations at each layer as outlined in Algorithm 2.